Synthesis of visible light-driven Eu, N co-doped TiO$_2$ and the mechanism of the degradation of salicylic acid

**Yunfei Ma · Jinlong Zhang · Baozhu Tian ·
Feng Chen · Shenyuan Bao · Masakazu Anpo**

Abstract   Europium and nitrogen co-doped TiO$_2$ was successfully synthesized by the precipitation–peptization method. The structure and properties of the catalysts were characterized by X-ray diffraction, transmission electron microscopy, X-ray photoelectron spectroscopy, and UV–vis diffuse reflectance spectra. The photocatalytic efficiency was evaluated by monitoring the photocatalytic degradation of salicylic acid under visible light irradiation. It was verified that TiO$_2$ co-doped with nitrogen and 1% europium showed the highest photocatalytic activity. The adsorption isotherms were obtained by measuring the salicylic acid concentration before and after the dark adsorption at different original solution concentrations. The results illustrated that the doping of Eu was beneficial to the adsorption of salicylic acid. The probable degradation mechanism of salicylic acid was examined by the addition of NaF, Na$_2$S$_2$O$_3$, and K$_2$S$_2$O$_8$ as the probe molecules. It was verified that salicylic acid was first adsorbed on the surface of the catalysts, followed by the degradation by the photogenerated holes (h_{vb}^{+}).

Keywords   Nitrogen · Europium · Co-doping · TiO$_2$ · Salicylic acid · Photocatalysis reaction

Y. Ma · J. Zhang (✉) · B. Tian · F. Chen · S. Bao
Key Laboratory for Advanced Materials and Institute of Fine Chemicals, East China University of Science and Technology, 130 Meilong Road, Shanghai 200237, People's Republic of China
e-mail: jlzhang@ecust.edu.cn

M. Anpo
Department of Applied Chemistry, Graduate School of Engineering, Osaka Prefecture University, Naka Ku 1-1 Gakuen-cho, Sakai, Osaka 599-8531, Japan

Introduction

Photocatalysis using TiO_2 as a catalyst has been widely reported as a promising technology for removal of various organic and inorganic pollutants from contaminated water and air because of its stability, low cost, and non-toxicity [1–4]. However, the widespread technological use of TiO_2 is impaired by its wide band gap (ca. 3.2 eV for crystalline anatase phase), the fast charge-carrier recombination, and the low interfacial charge-transfer rates [5]. Due to the above disadvantages, various approaches have been applied to enhance the photocatalytic activity under visible light illumination. Doping with nonmetals (such as N [6–9], S [10], C [11], and B [12, 13]) has been widely reported. Among them, N doping is the hottest topic. Asahi suggested that the N_2p level could mix with O_2p, which resulted in the narrowing of the band gap and enhancing of the photoactivity in the visible region [6]. Other researchers' work supported that the formation of localized midgap states above the top of the valence band by nitrogen doping was responsible for the visible photoactivity [14]. Transition metals (such as Fe [15, 16], V [17], W [18], Ag [19], Au [20], and Pt [21, 22]) are another kind of efficient dopant which can facilitate the charge separation and hence reduce the recombination of electrons and holes efficiently. Lanthanide ions, owing to their special 4f electron configuration, can form complexes with various Lewis bases including acids, amines, aldehydes, alcohols, and thiols. It is beneficial to the interfacial charge transfer to the contaminant [23]. So co-doping with rare earths and nonmetal was an efficient way to enhance the activity in the visible region. Shen et al. [24] synthesized titania co-doped with nitrogen and cerium by the sol–gel route. The as-prepared photocatalyst could absorb the visible light and showed high photoactivity in the visible region because of the band gap narrowing. Cong et al. [25] synthesized TiO_2 nanoparticles co-doped with nitrogen and lanthanum in a homogeneous precipitation–hydrothermal process. Some other researchers [26] have also reported rare earth and nitrogen co-doped TiO_2. All of them used the organic solvent or organic titanium precursor which is expensive or poisonous to our environment and health. Furthermore, sometimes annealing is indispensable to remove organic materials and reduce the effect of carbon on photoactivity. Calcination will also lead to the growth of the nanoparticle size, while doped nitrogen species may be removed under high temperature condition [27].

In this study, we prepared europium and nitrogen co-doped titanium dioxide (Eu/N–TiO_2) by the precipitation–peptization method, using inorganic titanium (titanium sulfate) as the titanium precursor. During the total synthesis process, no organic material was used. The dopant was dispersed homogeneously during the peptization process. In order to investigate the mechanism of photocatalytic reaction, adsorption isotherms were obtained which indicated that europium had a great effect on the adsorption ability. In principle, some valuable additional information on the mechanism of photocatalytic degradation of salicylic acid can be obtained by adding different probe molecules into the reaction systems. The addition of NaF illustrated that adsorption was a key step in the heterogeneous reaction. The important role of holes in the degradation of salicylic acid was confirmed by using $K_2S_2O_8$ as an electron acceptor and $Na_2S_2O_3$ as an efficient scavenger for holes.

Experimental

Materials

Titanium sulfate [$Ti(SO_4)_2$], ammonia ($NH_3 \cdot H_2O$), and nitric acid (HNO_3) were obtained from Shanghai Reagent. Salicylic acid (purity 99.5%) was purchased from Shanghai Lingfeng. Sodium fluoride (NaF), sodium hyposulfite ($Na_2S_2O_3$), and potassium peroxydisulfate ($K_2S_2O_8$) were purchased from Huadong Medicine, China. All chemicals were of analytical grade or higher and were used as received. Double-distilled water was used for all synthesis and treatment processes.

Samples preparation

Nine grams of $Ti(SO_4)_2$ was dissolved in 36 mL water under vigorous stirring. After that, an aqueous ammonia (30 wt%) solution was added dropwise until pH = 8.0. After aging in the mother liquid for 12 h, the precipitate obtained was suction-filtered and washed with double-distilled water until the removal of SO_4^{2-} (as was confirmed by the $BaCl_2$ test). The obtained precipitates were dispersed homogeneously in 60 mL water with different amounts of $Eu(NO_3)_3 \cdot 6H_2O$, adjusting the pH of solution with HNO_3 up to a certain value. The precipitates were peptized at 60 °C under continual magnetic stirring, and a transparent sol was formed after about 2 h. The sol was poured onto a plate and dried with water vapor. Eu, N co-doped TiO_2 was obtained after the gel annealed at 300 °C for 2 h. The pure TiO_2 was obtained by the addition of a 12-M NaOH solution instead of ammonia solution during the precipitation process, and HCl was used to adjust the pH value during the peptization process.

Characterizations

X-ray diffraction (XRD) patterns of all samples were collected in the range 10–80° with a stepwidth of $0.02° \ s^{-1}$ using a Rigaku D/MAX 2550 VB/PC apparatus (Cu Kα radiation, $\lambda = 1.5406$ Å), operated at 40 kV and 100 mA. The surface morphologies and particle sizes were observed by transmission electron microscopy (TEM, JEM-2011), using an accelerating voltage of 200 kV. The samples were prepared by grinding and subsequently dispersing the powder in acetone and applying a drop of very dilute suspension on carbon-coated grids. The UV–vis absorbance spectra were obtained for the dry-pressed disk samples using a Scan UV–vis spectrophotometer (Varian, Cary 500) equipped with an integrating sphere assembly, using $BaSO_4$ as the reflectance sample. The spectra were recorded at room temperature in air within the range 200–800 nm. To investigate the chemical states of the photocatalyst, X-ray photoelectron spectroscopy (XPS) was recorded with Perkin Elmer PHI 5000C ESCA System with Al Kα radiation operated at 250 W. The shift of the binding energy due to relative surface charging was corrected using the C1 s as an internal standard at 284.6 eV.

Evaluation of photocatalytic activity

The photocatalytic activity was evaluated by measuring the decomposition of 50 mg/L salicylic acid solution. A 1,000-W tungsten halogen lamp was used as the light source, surrounded with a water circulation facility at the outer wall through a quartz jacket. The short wavelength components (λ <420 nm) of the light were cut off using UV cut-off filters. The distance between the lamp and the center of the quartz tube was 10 cm. For a typical photocatalytic experiment, 50 mg of catalyst powder was added to 50 mL of the above salicylic acid solution in the quartz tube. The initial pH value of the solution was kept at 3.5. Prior to irradiation, the suspensions were magnetically stirred in the dark for 30 min to ensure the establishment of an adsorption/desorption equilibrium. The above suspensions were kept under air-equilibrated conditions before and during the irradiation. After specific intervals, about 4 mL liquid was taken and centrifuged. The supernatant liquid was analyzed by recording the absorbance at 297 nm of salicylic acid solution using a UV–vis spectrophotometer (Varian, Cary 100). According to the standard curve of concentration and absorption, the value of $\Delta C/C_0$ was calculated which indicated the decomposition efficiency.

In the experiment requiring scavengers, different amounts of probe molecules (NaF, $K_2S_2O_8$, and $Na_2S_2O_3$) were added to the salicylic acid solution before the introduction of the 1.0% Eu/N–TiO$_2$ as the catalyst. The rest of the procedure was the same as the above photoactivity evaluation.

Adsorption isotherm measurement

The adsorption behavior of various samples to salicylic acid was carried out in dark. An amount of 30 mg catalyst was added into 30 mL salicylic acid solution with different initial concentration. After 30 min stirring, the concentration of salicylic acid was found to be constant. The adsorbed amount of salicylic acid on sample with different initial solutions was obtained by comparing the original concentration and the equilibrium concentration.

Results and discussion

Crystal structure

Figure 1 shows the XRD patterns in the 2θ region from 10 to 80° for pure TiO$_2$ and Eu, N co-doped TiO$_2$ calcined at 300 °C. The patterns show that all samples contain a little brookite structure but are dominated by anatase. The diffraction peaks due to the TiO$_2$ anatase in the samples become broader and weaker with increasing amounts of Eu. This indicates that, with the increase of Eu dosage, the crystallinity of the TiO$_2$ anatase phase deteriorates and the crystallite size of the TiO$_2$ anatase becomes smaller.

From the (101) diffraction peak of anatase TiO$_2$, the average crystallite sizes of TiO$_2$ anatase can be calculated from the Debye–Scherrer equation. The results are
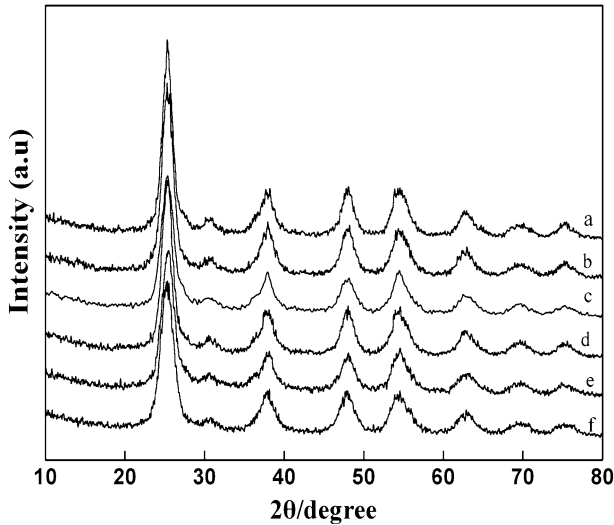
Fig. 1 XRD patterns of pure TiO_2 and N–TiO_2 doped with different amounts of Eu: **a** pure TiO_2, **b** N–TiO_2, **c** 0. 5% Eu/N–TiO_2, **d** 1.0% Eu/N–TiO_2, **e** 1.5 Eu%/N–TiO_2, **f** 2.0% Eu/N–TiO_2

summarized in Table 1. It can be seen that the average crystallite size decreased from 7.5 nm (pure TiO_2) to 5.4 nm (2% Eu/N–TiO_2). TiO_2 has a tetragonal structure, whose unit cell parameters can be calculated according to Eqs. 1 and 2:

$$d_{(hkl)} = \lambda/2 \sin \theta \tag{1}$$

$$1/d_{hkl}^2 = h^2/a^2 + k^2/b^2 + l^2/c^2. \tag{2}$$

In this study, the diffraction peaks from (101) to (200) planes of TiO_2 anatase were employed to calculate the unit cell parameters of TiO_2 anatase. Table 1 shows the unit cell parameters of TiO_2 anatase calculated from the XRD data. The unit cell parameters of TiO_2 anatase do not change much from the pure TiO_2 to Eu/N–TiO_2. This means Eu^{3+} did not enter the TiO_2 matrix. Generally, the ionic radius of Eu^{3+} (0.95 Å) is larger than that of Ti^{4+} (0.68 Å), and Eu^{3+} can hardly enter the lattice of TiO_2 [28], but the highly dispersed rare earths inhibit grain growth by restricting the coalescence of some smaller neighboring grains.

Table 1 Lattice parameters, cell volume, and crystal size of different samples

Samples	$a = b$ (Å)	c (Å)	Cell volume (Å^3)	Crystal size (nm)
Pure TiO_2	3.782	9.570	136.9	7.53
N–TiO_2	3.773	9.605	136.7	7.06
0.5 Eu–N/TiO_2	3.773	9.608	136.8	6.65
1.0 Eu–N/TiO_2	3.786	9.471	135.8	6.48
1.5 Eu–N/TiO_2	3.783	9.487	135.8	6.36
2 .0 Eu–N/TiO_2	3.793	9.425	135.6	5.44

TEM analysis

The TEM and HRTEM images of 1.0% Eu/N–TiO$_2$ calcined at 300 °C are shown in Fig. 2. During the calcination, europium nitrate was converted into Eu$_2$O$_3$ and deposited onto the surface of N–TiO$_2$. Figure 2a shows that the prepared sample has a small crystallite size of around 6 nm in diameter, which is in accordance with the XRD result. Figure 2b shows part of one nanocrystal having several lattice planes. The d-spacing of 0.352 nm corresponding to the distance between the (101) planes is the characteristic lattice fringes of the anatase TiO$_2$ crystal. Figure 2c presents the selected area electron diffraction and lattice fringes. This result further proves that the crystallite is dominated by the anatase phase and with high uniform morphology.
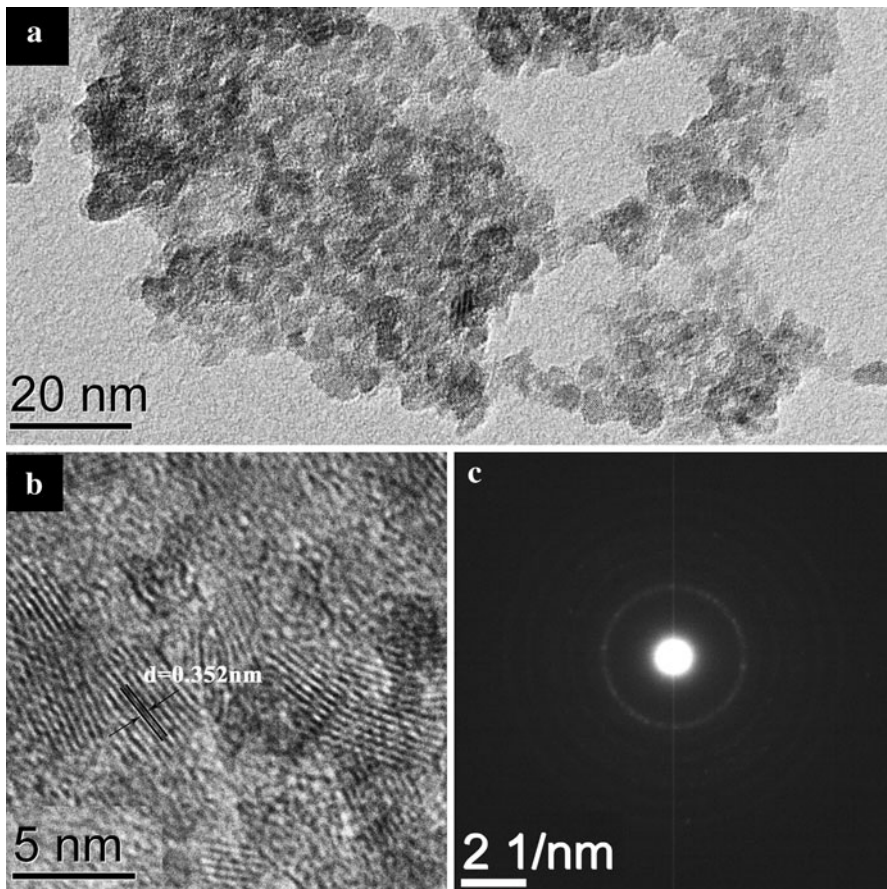

Fig. 2 TEM and HRTEM of 1.0% Eu/N–TiO$_2$

UV–vis absorbance spectra

Figure 3a presents the UV–vis absorption spectra of the prepared samples. With the doping of nitrogen, there is a red shift toward the visible region. Figure 3b shows the $(\alpha h v)^{1/2}$ versus energy of light for direct band gap transition of pure TiO_2 and modified TiO_2. The band gap of pure TiO_2 is 3.1 eV, and the band gap of $N–TiO_2$ and 1.0% $Eu/N–TiO_2$ is 2.8 and 2.75 eV, respectively.

XPS analysis

XPS is known as a particle surface analysis technique. In XPS, excitation by X-rays allows core atomic levels to be probed, and the resultant chemical shift provides an indication of the oxidation state of the material on the surface. Carbon is always present in XPS as a result of hydrocarbon deposits in air and/or vacuum, which is commonly used as an internal energy calibrated at 284.6 eV. The XPS spectra of Ti2p, O1s, N1s, and Eu4d of 1.0% $Eu/N–TiO_2$ are presented in Fig. 4. The spectrum of Ti in Fig. 4A shows two well-resolved peaks. One of them is centered at 458.2 eV, while the other is centered at 463.9 eV. The peaks are due to the Ti^{4+} ions in titania assigned to $Ti(2p_{3/2})$ and $Ti(2p_{1/2})$ states, respectively. But for pure anatase TiO_2, peaks for $Ti(2p_{3/2})$ and $Ti(2p_{1/2})$ states are at 458.6 and 464.3 eV, respectively [29]. The position of Ti2p was shifted to lower binding energy compared with pure anatase TiO_2. This result indicated that the doping of nitrogen has an effect on the surrounding electron. Partial electrons transferred from the N to the Ti and the O, due to the lower electronegativity of nitrogen compared with oxygen. Therefore, the electron density of Ti increased and the binding energy decreased. This result is in agreement with other researchers [8, 30].

The shape of the O1s XPS spectrum in Fig. 4B indicates that it is composed of two peaks. One is centered at 529.9 eV, which is due to the contribution of oxygen atoms from metal oxide, e.g., from titanium dioxide and europium dioxide. The presence of additional broad photoelectron peak at the higher binding energy range
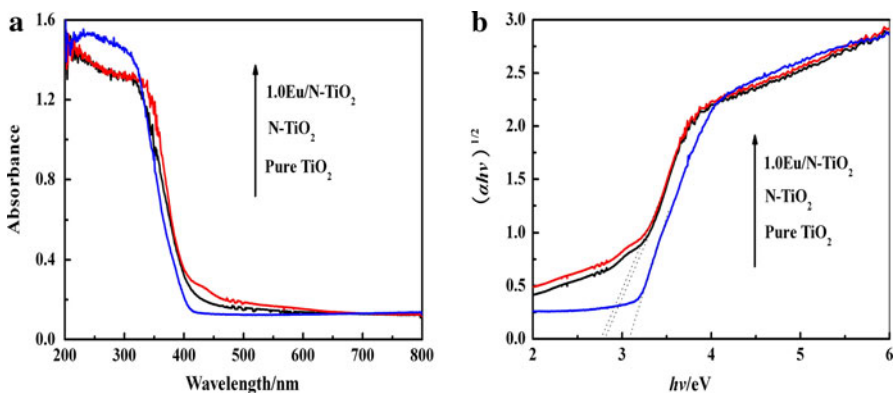

Fig. 3 (a) UV-vis spectra and (b) plot of transformed Kubelka-Munk function versus the energy of the light absorbed of different samples
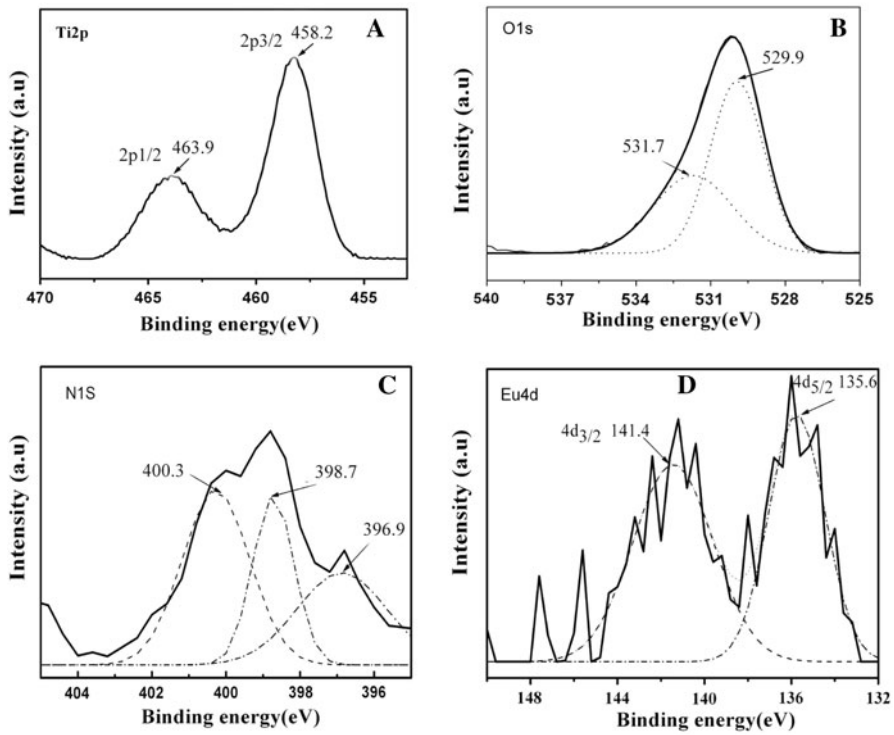
Fig. 4 XPS spectra of 1.0% Eu/N–TiO$_2$

was centered at 531.7 eV. This peak could be attributed to the hydroxyl group. It is reported that the hydroxyl group measured by XPS is ascribed to the water chemisorbed on the surface of titanium dioxide [31, 32]. This indicates that the doping of Eu enhances hydrophilic properties of the sample.

As for the N1s XPS spectrum, previous studies have shown the typical binding energy of nitrogen in TiN and NaNO$_3$ at 397.2 and 408 eV [33], respectively. In this work, the N1s XPS spectrum can be fitted to three kinds of chemical states using multi-peak Gaussian approximation (Fig. 4C). The peak at 396.9 eV can be assigned to the formation of N–Ti–N [6, 34, 35]. In addition, two small peaks are observed at 398.7 and 400.3 eV. As is well known, the element adjacent to nitrogen directly influences its binding energy. The stronger the electronegativity of the adjacent element, the higher the binding energy of nitrogen. We attribute the peak at 398.7 eV to the N atom in the environment of O–Ti–N. The peak at 400.3 eV is the N atom in the environment of Ti–O–N. The analysis of the N1s XPS confirmed that nitrogen atoms were successfully doped into TiO$_2$, and some substituted the sites of oxygen atoms.

For the spectrum of Eu4d in Fig. 4D, the prominent peak around 135.6 eV can be assigned to the Eu^{3+}4d$_{5/2}$ configuration. The other spin–orbit component, the 4d$_{3/2}$ appears at 141.4 eV. The two-component separation is 5.8 eV, which is in good agreement with other measurements [36]. The signal of Eu4d suggests the presence of Eu$_2$O$_3$ in sample.

Photocatalytic activity

The photocatalytic activity of pure TiO_2 and $N–TiO_2$ doped with different amount of europium are shown in Fig. 5. It can be seen that the europium-doped $N–TiO_2$ has better activity than the pure TiO_2. A better and more quantitative method of presenting the activities of the samples is the use of the rate constant k, while k is calculated according to the following equation:

$$\ln C_0/C_t = kt. \tag{3}$$

where C_0 and C_t represent initial equilibrium concentration and the reaction concentration of salicylic acid, respectively. In photocatalysis reaction, k is almost independent of the temperature and concentration used because the photoactivtion process depends only on the radiant flux and on the visible light spectrum of the lamp. The reaction kinetics of different samples are shown in Fig. 6, and the rate constants are listed in Table 2. The rate constant k of pure TiO_2 is 0.0005 min^{-1} and the degradation is 14%. For the pure TiO_2, the catalyst turned pale yellow upon immersion in salicylic acid solutions which are photosensitive and lead to degrading by pure TiO_2 [23]. With the doping of nitrogen, the rate constant k of $N–TiO_2$ is 0.0026 min^{-1} with a degradation of 54%. The enhancement in the degradation of salicylic acid is attributed to absorption in the visible light region by the doped nitrogen species. With the increase of the europium dosage, the photocatalytic activity increased initially, but decreased when the doping content of europium was higher than 1%. Obviously, 1.0% $Eu/N–TiO_2$ achieved the best photocatalytic performance with k of 0.0064 min^{-1} and the highest degradation of 88%. This might be due to the fact that there was an optimum doping content in the TiO_2 particles for the most efficient separation of photoinduced electron–hole pairs.
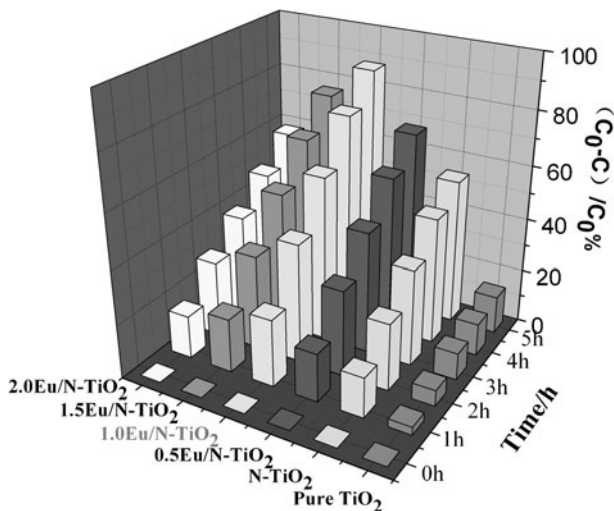

Fig. 5 Degradation of salicylic acid (50 mg/L) by pure TiO_2 and $N–TiO_2$ doped with different amounts of Eu
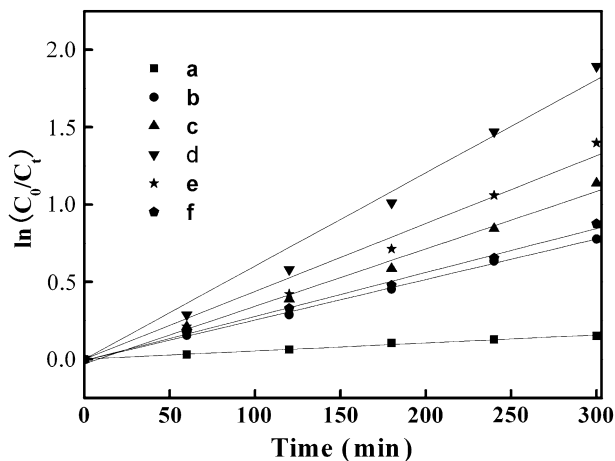
Fig. 6 Reaction kinetic of pure TiO$_2$ and N–TiO$_2$ doped with different amount of Eu: **a** pure TiO$_2$, **b** N–TiO$_2$, **c** 0.5% Eu/N–TiO$_2$, **d** 1.0% Eu/N–TiO$_2$, **e** 1.5% Eu/N–TiO$_2$, **f** 2% Eu/N–TiO$_2$

Table 2 The first-order kinetic constants (k, min^{-1}) and relative coefficient (R^2) of different samples for degradation of salicylic acid under visible light irradiation

Photocatalysts	K (min^{-1})	R^2	Degradation %
Pure TiO$_2$	0.0005	0.9905	14
N–TiO$_2$	0.0026	0.9983	54
0.5 Eu–N/TiO$_2$	0.0037	0.9908	68
1.0 Eu–N/TiO$_2$	0.0064	0.9905	88
1.5 Eu–N/TiO$_2$	0.0047	0.9875	76
2.0 Eu–N/TiO$_2$	0.0028	0.9955	58

Mechanism of the degradation of the salicylic acid

Adsorption behavior

In heterogeneous catalytic reaction, adsorption and desorption of reactants and intermediates have great influence on the efficiency of the overall degradation process. Organic compounds chemisorbed on TiO$_2$ surface directly react with photogenerated holes, while reactant dissolved in aqueous environment are generally attacked by radicals such as ·OH, or O$_2^-$ on the surface or in the bulk of aqueous phase. Thus, adsorption experiments are considered as essential for a detailed study in this field. In this experiment, adsorption behavior was investigated by a set of adsorption experiments, as shown in Fig. 7. The adsorption isotherms of salicylic acid can be analyzed by Langmuir adsorption model:

$$C_e/Q_e = 1/Q_{max}K_a + C_e/Q_{max} \qquad (4)$$

where C_e is the concentration of the salicylic acid in the solution at equilibrium (mmol/L), Q_e is the adsorption amount in the solution at equilibrium (mmol/g). K_a is
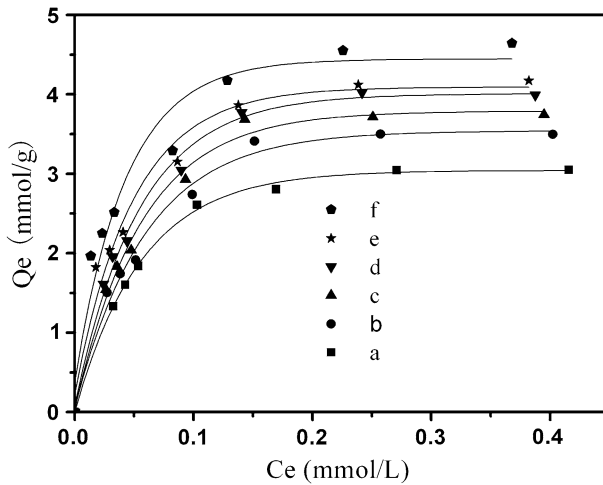
Fig. 7 Adsoption isotherms of pure TiO_2 and N–TiO_2 doped with different amounts of Eu: **a** pure TiO_2, **b** N–TiO_2, **c** 0. 5% Eu/N–TiO_2, **d** 1.0% Eu/N–TiO_2, **e** 1.5% Eu/N–TiO_2, **f** 2% Eu/N–TiO_2

the Langmuir adsorption equilibrium constant (L/mmol). Q_{max} is the saturated adsorption amount (mmol/g). The plot of C_e/Q_e versus C_e would give a straight line, and then Q_{max} and K_a can be derived from the slope and the intercept of the plot. The correlation coefficient R represents the conformity between the experimental results and the Langmuir adsorption isotherm model. According to the adsorption experimental data of salicylic acid on different catalysts, K_a, Q_{max} and the correlation coefficient are obtained and presented in Table 3.

The results indicate that the adsorption equilibrium constants (K_a) of Eu, N co-doped TiO_2 catalysts are much higher than that of the pure TiO_2 catalyst, and Q_{max} are also higher than that of the pure TiO_2 catalyst. The factors that led to the enhanced adsorption capacity should involve the change of the physical or chemical properties of the catalysts owing to Eu ion doping. From Table 1, it can be seen that, with the increase of the dopant of Eu, the crystallite size decreased. The smaller crystal size and larger specific surface area of TiO_2 catalysts would result in better physical adsorption of salicylic acid. Moreover, it was reported that rare earth ions

Table 3 Langmuir adsorption equilibrium constant (K_a L/mmol) and saturated adsorption amount (Q_{max} mmol/g) for salicylic acid on catalysts

Dosage (%)	K_a (L/mmol)	Q_{max} (mmol/g)	R^2
N–TiO_2	23.1032	3.4352	0.9967
0.25 Eu/N–TiO_2	23.4953	3.9777	0.9938
0.5 Eu/N–TiO_2	23.8282	4.2391	0.9939
1.0 Eu/N–TiO_2	24.555	4.5249	0.9958
1.5 Eu/N–TiO_2	29.4054	4.5956	0.9974
2.0 Eu/N–TiO_2	33.61	5.0429	0.9968

can coordinate with salicylic acid for its special 4f electron configuration [27]. The adsorption equilibrium constant for the formation of Ti^{4+}-salicylic acid is estimated to be $K = 2.2 \times 10^2$ which is lower than that of Ln^{3+}-salicylic acid $K = 5.0 \times 10^2$ [23]. Therefore, the modified TiO_2 has a stronger adsorption ability than the pure TiO_2.

Effect of different probe molecules on the photocatalytic activity

In order to further illustrate the effect of adsorption on the photocatalytic activity, different amounts of NaF were added to the reaction solution. The degradation of salicylic acid with different amounts of NaF are shown in Fig. 8a. When there is no NaF, the degradation of salicylic acid by the 1.0% Eu/N–TiO_2 under visible light irradiation is 88%. With the molar ratio of NaF to salicylic acid increased from 1:1 to 10:1, the degradation decreased from 61 to 13%. This can be explained by F^- having a stronger adsorption ability on the surface of TiO_2 catalysts than the salicylic acid. Thus, the surface of the catalyst was dominated by F^-. The rate of degradation of salicylic acid is greatly inhibited by the presence of NaF. Thus, it can be concluded that the preferential adsorption on the surface of catalyst is a crucial step in this photocatalytic reaction.

The effect of the addition of $K_2S_2O_8$ on the photocatalytic activity is shown in Fig. 8b. With the addition of $K_2S_2O_8$, the photocatalytic activity noticeably
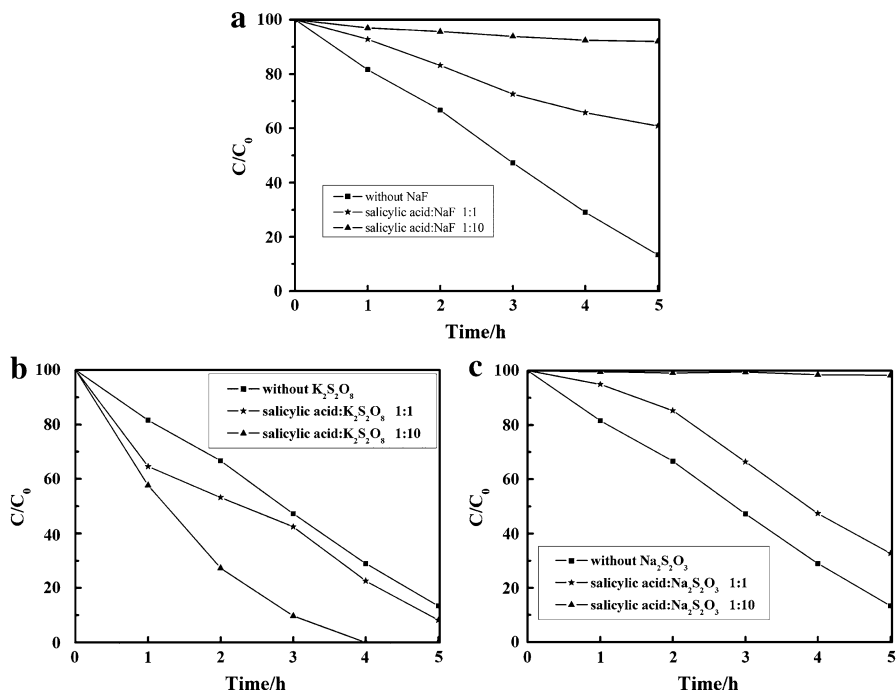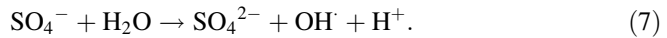

Fig. 8 Effect of the addition of different probe molecule on the degradation of salicylic acid by 1% Eu/N–TiO_2: **a** NaF, **b** $K_2S_2O_8$, **c** $Na_2S_2O_3$

increased. When the molar ratio of $K_2S_2O_8$ to salicylic acid was 10:1, the degradation of salicylic acid was 91% after being irradiated for 3 h. As a kind of strong electron acceptor, the persulphate ions are known to capture the photogenerated electrons quickly and to generate hydroxyl radicals by the mechanisms shown in Eqs. 5–7:

$$TiO_2 + h\upsilon \rightarrow h^+ + e^- \tag{5}$$

$$S_2O_8{}^{2-} + e_{cb}^- \rightarrow SO_4{}^{2-} + SO_4^- \tag{6}$$

$$SO_4^- + H_2O \rightarrow SO_4{}^{2-} + OH^. + H^+. \tag{7}$$

The respective one-electron reduction potentials of different species are: $E(O_2/O_2^-) = -155$ mV, $E(S_2O_8{}^{2-}/SO_4^-) = 1{,}100$ mV [37], From the thermodynamic point of view, the persulphate ion is a more efficient electron acceptor than molecular oxygen. So the addition of $K_2S_2O_8$ reduces the recombination of electrons and holes, thus greatly enhancing the photocatalytic activity. The effect of $K_2S_2O_8$ on the photoactivity has also been observed in a number of previous studies [38–40].

Figure 8c shows that the photocatalytic degradation of salicylic acid was strongly inhibited by the addition of $Na_2S_2O_3$. The degradation of salicylic acid decreased from 88 to 68 and to 2% with the presence of molar ratios of salicylic acid to $Na_2S_2O_3$ of 1:1 and 1:10. This is because $Na_2S_2O_3$ is a strong reducing agent and can readily react with valance band holes (h_{vb}^+) [41, 42]. It was oxidized to $SO_3{}^{2-}$ and subsequently to $S_2O_6{}^{2-}$. The process can be summarized as Eqs. 8 and 9.

$$S_2O_3{}^{2-} + 4h^+ + 6OH^- \rightarrow 2SO_3{}^{2-} + 3H_2O \tag{8}$$

$$2SO_3{}^{2-} + 2h^+ \rightarrow S_2O_6{}^{2-}. \tag{9}$$
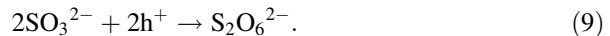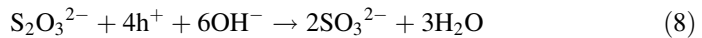
From the above, it can be concluded that salicylic acid was adsorbed on the surface of the catalysts and oxidized under the effect of holes. The h_{vb}^+ has an important role in the degradation of salicylic acid.

Conclusions

The present study demonstrated that titanium dioxide co-doped with europium and nitrogen with high visible light catalytic activity was successfully synthesized by inorganic chemicals. The doped nitrogen extended the absorption to the visible region, and the doped europium increased the adsorption ability to the salicylic acid. An amount of 1.0% $Eu/N–TiO_2$ exhibited the best catalytic activity. Various probe molecules were added to the reaction system to explore the reaction mechanism. It can be deduced that the contaminants were first adsorbed on the surface of the catalyst, and were then decomposed quickly under the effect of the holes.

References

1. T.X. Liu, F.B. Li, X.Z. Li, J. Hazard. Mater. **152**, 347 (2008)
2. J. Grzechulska, A.W. Morawski, Appl. Catal. B Environ. **36**, 45 (2002)
3. C. Young, T.M. Lim, K. Chiang, J. Scott, R. Amal, Appl. Catal. B Environ. **78**, 1 (2008)
4. M.R. Hoffmann, S.T. Martin, W. Choi, D.W. Bahnemann, Chem. Rev. **95**, 69 (1995)
5. W. Balcerski, S.Y. Ryu, M.R. Hoffmann, J. Phys. Chem. C **111**, 15357 (2007)
6. R. Asahi, T. Morikawa, T. Ohwaki, K. Aoki, Y. Taga, Science **293**, 269 (2001)
7. Y. Cong, J.L. Zhang, F. Chen, M. Anpo, J. Phys. Chem. C **111**, 6976 (2007)
8. M. Sathish, B. Viswanathan, R. Viswanath, C. Gopinath, Chem. Mater. **17**, 6349 (2005)
9. Y.M. Wu, M.Y. Xing, B.Z. Tian, J.L. Zhang, F. Chen, Chem. Eng. J. **162**, 710 (2010)
10. T. Umebayashi, T. Yamaki, S. Yamamoto, A. Miyashita, S. Tanaka, T. Sumita, K. Asai, J. Appl. Phys. **93**, 5156–5160 (2003)
11. Y.M. Wu, J.L. Zhang, L. Xiao, F. Chen, Appl. Surf. Sci. **256**, 4260 (2010)
12. Y.M. Wu, M.Y. Xing, J.L. Zhang, F. Chen, Appl. Catal. B Environ. **97**, 182 (2010)
13. A. Zaleska, E. Grabowska, J.W. Sobczak, M. Gazda, J. Hupka, Appl. Catal. B Environ. **89**, 469 (2009)
14. C. Di Valentin, G. Pacchioni, A. Selloni, S. Livraghi, E. Giamello, J. Phys. Chem. B **109**, 11414 (2005)
15. H.K. Shon, D.L. Cho, S.H. Na, J.B. Kim, H.-J. Park, J.H. Kim, J. Ind. Eng. Chem. **15**, 476 (2009)
16. J.F. Zhu, W. Zheng, J.L. Zhang, M. Anpo, J. Mol. Catal. A Chem. **216**, 35 (2004)
17. B.Z. Tian, C.Z. Li, F. Gu, H.B. Jiang, Y.J. Hu, J.L. Zhang, Chem. Eng. J. **151**, 220 (2009)
18. S.A.K. Leghari, S. Sajjad, F. Chen, J.L. Zhang, Chem. Eng. J. **166**, 906 (2010)
19. V. Vamathevan, R. Amal, D. Beydoun, G. Low, S. McEvoy, J. Photochem. Photobiol. A. Chem. **148**, 233 (2002)
20. Y.M. Wu, J.L. Zhang, L. Xiao, F. Chen, Appl. Catal. B Environ. **88**, 525 (2009)
21. M. Qamar, Desalination **254**, 108 (2010)
22. L. Shivalingappa, J. Sheng, T. Fukami, Vacuum **48**, 413 (1997)
23. K.T. Ranjit, I. Willner, S.H. Bossmann, A.M. Braun, J. Catal. **204**, 305 (2001)
24. X.Z. Shen, Z.C. Liu, S.M. Xie, J. Guo, J. Hazard. Mater. **162**, 1193 (2009)
25. Y. Cong, B.Z. Tian, J.L. Zhang, Appl. Catal. B Environ **101**, 376 (2011)
26. D.G. Huang, S.J. Liao, W.B. Zhou, S.Q. Quan, L. Liu, Z.J. He, J.B. Wan, J. Phys. Chem. Solids **70**, 853 (2009)
27. Y.F. Ma, J.L. Zhang, B.Z. Tian, F. Chen, L.Z. Wang, J. Hazard. Mater. **182**, 386 (2010)
28. J. Lin, J.C. Yu, J. Photochem. Photobio. A Chem. **116**, 63 (1998)
29. Y. Li, D.-S. Hwang, N.H. Lee, S.-J. Kim, Chem. Phys. Lett. **404**, 25 (2005)
30. X. Chen, C. Burda, J. Phys. Chem. B **108**, 15446 (2004)
31. P.M. Kumar, S. Badrinarayanan, M. Sastry, Thin Solid Films **358**, 122 (2000)
32. H. Perron, J. Vandenborre, C. Domain, R. Drot, J. Roques, E. Simoni, J.J. Ehrhardt, H. Catalette, Surf. Sci. **601**, 518 (2007)
33. X. Chen, Y.B. Lou, A. Samia, C. Burda, J. Gole, Adv. Funct. Mater. **15**, 41 (2005)
34. H. Irie, Y. Watanabe, K. Hashimoto, J. Phys. Chem. B **107**, 5483 (2003)
35. J.L. Gole, J.D. Stout, C. Burda, Y. Lou, X. Chen, J. Phys. Chem. B **108**, 1230 (2003)
36. C.S. Fadley, D.A. Shirley, Phys. Rev. A **2**, 1109 (1970)
37. P. Wardman, J. Phys. Chem. Ref. Data **18**, 1637 (1989)
38. S. Qourzal, N. Barka, M. Tamimi, A. Assabbane, Y. Ait-Ichou, Appl. Catal. A **334**, 386 (2008)
39. S. Yamazaki, S. Matsunaga, K. Hori, Water Res. **35**, 1022 (2001)
40. A. Mills, M.A. Valenzuela, J. Photochem. Photobio. A Chem **165**, 25 (2004)
41. S. Boumaza, A. Boudjemaa, A. Bouguelia, R. Bouarab, M. Trari, Appl. Energy **87**, 2230 (2010)
42. S. Boumaza, R. Bouarab, M. Trari, A. Bouguelia, Energy Convers. Manage. **50**, 62 (2009)